Pergamon

Geochimica et Cosmochimica Acta, Vol. 61, No. 24, pp. 5279–5293, 1997

0016-7037/97 $17.00 + .00

PII S0016-7037(97)00317-7

Gibbs free energies of formation of RuO_2, IrO_2, and OsO_2: A high-temperature electrochemical and calorimetric study

Hugh St.C. O'Neill* and Johan Nell†

Bayerisches Geoinstitut, Universität Bayreuth, D-95440 Bayreuth, Germany

(*Received May* 21, 1997; *accepted in revised form August* 27, 1997)

Abstract—The Gibbs free energies of formation of RuO_2, OsO_2 and IrO_2 have been determined by measuring the chemical potentials of oxygen (μO_2) defined by the reactions $M + O_2 = MO_2$, where M = Ru, Os. or Ir, using an electrochemical method with calcia-stabilized zirconia (CSZ) solid electrolytes. Measurements were attempted in the temperature ranges from ~870 K to 1620, 1270, and 1415 K for the Ru, Os, and Ir equilibria, respectively, but inspection of the results reveals that equilibrium could not be established below ~930 K for all three reactions. For Ru + RuO_2, the highest temperature data (above 1520 K) may be systematically affected by the onset of significant electronic conduction in the CSZ electrolyte, while the attempted measurements of the Os + OsO_2 equilibrium above 1190 K are obscured by the disproportionation of OsO_2 to gaseous Os oxides.

The high temperature heat capacities at constant pressure (C_p) of RuO_2 and IrO_2 were determined from 370 to 1070 K by differential scanning calorimetry. These data were combined with heat content measurements and low-temperature heat capacities from the literature, and fitted to an extended Maier-Kelley equation. The calorimetric data for RuO_2 and IrO_2, together with assessed data for Ru, Os, and Ir metals and estimated data for OsO_2, were used in a third law analysis of the electrochemical measurements.

The values of μO_2 of the three equilibria were smoothed and filtered by the third-law analysis to yield the following equations which can be extrapolated to lower and higher temperatures as indicated:

$$\mu O_2\,(Ru + RuO_2) = -324563 + 344.151\,T - 22.1155\,T \ln T \quad (700 < T < 1800)$$
$$\mu O_2\,(Os + OsO_2) = -300399 + 307.639\,T - 17.4819\,T \ln T \quad (700 < T < 1500)$$
$$\mu O_2\,(Ir + IrO_2) = -256518 + 295.854\,T - 15.2368\,T \ln T \quad (700 < T < 1500)$$

where μO_2 is in J mol^{-1}, T is in K, the reference pressure for O_2 is 1 bar (10^5 Pa), and estimated accuracies are approximately 200 to 400 J mol^{-1}. For Ru + RuO_2, the drift in the measurements relative to the calorimetric data deduced from the third-law evaluation is 0.7 J K^{-1} mol^{-1}, and for Ir + IrO_2 is 1.6 J K^{-1} mol^{-1}. The analogous third-law evaluation of the Os + OsO_2 data gives $S^\circ_{298K} = 54.8 \pm 0.7$ J K^{-1} mol^{-1} and $\Delta_f H^\circ_{298K} = -291.8 \pm 0.6$ *kJ mol*$^{-1}$ for OsO_2.

1. INTRODUCTION

There is considerable geological interest in the Platinum Group Elements (PGEs: Ru, Rh, Pd, Os, Ir, Pt), not only because of their economic importance, but also because their distinctive geochemical properties can illuminate geological processes from a different angle than that offered by the more traditionally studied lithophile trace elements. An example is the way in which Os isotopes are shedding light on crust/mantle differentiation. Despite this, our quantitative understanding of the geochemical behaviour of the PGEs is still quite poor. For example, recent experimentally based estimates of the partitioning of Ir and Pt between silicate melt and Fe-rich metal or sulfide differ by up to 8 orders of magnitude (see O'Neill et al., 1995). Resolution of these discrepancies requires a thorough understanding of the thermochemical basis of the geochemical properties of the PGEs.

Here we report new experimental data on the thermochemical properties of RuO_2, OsO_2, and IrO_2. These rutile-structured dioxides are the lowest-valence oxides of their respective metals which are stable at high temperatures, and as such make convenient standard states from which to describe the thermochemochemical behaviour of oxidized forms of Ru, Os, and Ir in naturally occurring oxides, silicates, and silicate melts (e.g., O'Neill et al., 1995). The free energies of formation of these oxides were measured electrochemically from the reactions:

$$Ru + O_2 = RuO_2 \quad (1)$$

$$Os + O_2 = OsO_2 \quad (2)$$

$$Ir + O_2 = IrO_2 \quad (3)$$

using a high-temperature electrochemical method with oxygen-specific CSZ (calcia-stabilized zirconia) solid electrolytes. In addition, we have measured the heat capacities at constant pressure (C_p) of RuO_2 and IrO_2 in the range 370 to 1070 K by differential scanning calorimetry. The heat capacity data, when combined with literature data for calorimetrically determined entropies at 298.15 K (S°_{298K}) of RuO_2 and IrO_2 and the entropies and heat capacities of Ru and Ir metals and O_2 gas, permit third-law evaluations of the

**Present address*: Research School of Earth Sciences, Australian National University, Canberra ACT 0200, Australia (hugh.oneill@anu.edu.au).

†*Present address*: Mineralogy and Process Chemistry Division, Mintek Private Bag X3015, Randburg 2125, South Africa.

Table 1. Previous studies of the Gibbs free energies of formation of RuO_2, OsO_2, and IrO_2.

Reference	Method	Temperature range (K)
	RuO_2	
Schäfer et al. (1963)	p_{O_2} of oxidation of Ru	1377–1451
	O_2 dissociation pressure	1173–1523
Bell and Tagami (1963)	O_2 dissociation pressure	1380–1776
Kleykamp (1969)	EMF vs. Fe-"FeO"	780–1040
Pizzini and Rossi (1971)	EMF vs. air	750–1250
Chatterji and Vest (1971)	EMF vs. Cu-Cu_2O	873–1273
Tagirov et al. (1975)	O_2 dissociation pressure	1000–1200
Cordfunke and Konings (1988)	EMF vs. air and O_2	940–1077
Mallika and Sreedharan (1990)	EMF vs. air and Cu-Cu_2O	751–1200
	OsO_2	
Franco and Kleykamp (1972)	EMF vs. Fe-"FeO"	840–1070
	IrO_2	
Schäfer and Heitland (1960)	gas phase equilibria	1100–1400
Cordfunke and Meyer (1962)	O_2 dissociation pressure	1144–1298
Bell et al. (1966)	O_2 dissociation pressure	1201–1379
Kleykamp and Paneth (1973)	EMF vs. Fe-"FeO"	900–1200
Ramakrishnan et al. (1975)	EMF vs. Ni-NiO and Cu-Cu_2O	920–1136
Cordfunke (1981)	O_2 dissociation pressure	1115–1271
	EMF vs. O_2	937–1221
Mallika et al. (1985)	EMF vs. air	762–1260

electrochemical results and derivation of the standard enthalpies of formation ($\Delta_f H^\circ_{298K}$, equivalent to the enthalpy of reaction for reactions 1 and 3) of RuO_2 and IrO_2, from the relationship:

$$\Delta_r H^\circ_{298K} = \Delta_r G^\circ_T - \int_{298}^{T} \Delta_r C^\circ_p \cdot dT + T\,\Delta_r S^\circ_{298K} + T \int_{298}^{T} \Delta_r C^\circ_p / T \cdot dT \quad (4)$$

Estimated heat capacities for OsO_2 have been used in an analogous exercise to determine the enthalpy of formation and entropy of OsO_2 at 298.15 K.

The electrochemical method is capable of high precision and accuracy (O'Neill and Pownceby, 1993) and is very well suited for studying the Ru and Ir equilibria. It is not surprising, therefore, that several previous electrochemical studies on these two equilibria have been made (see Table 1). However, the reported precision of most of these studies is only of the order of ± 1 kJ mol^{-1} in μO_2, or worse. The exceptions are the studies of Cordfunke (1981) and Cordfunke and Konings (1988); current experimental practice should enable precise and accurate measurements to much better than this (say, ± 0.2 kJ mol^{-1}). There are also considerable differences among the results of these previous studies, which are far larger even than the rather disappointing precision (this will become apparent when we compare our results to the previous work). The Os equilibrium poses special experimental problems due to the stability of high-valence gaseous oxides of Os, which results in disproportionation of OsO_2 at moderate temperatures, according to the reactions:

$$2\ OsO_2 = Os + OsO_{4(gas)} \quad (5a)$$

$$3\ OsO_2 = Os + 2\ OsO_{3(gas)} \quad (5b)$$

(e.g., Nikol'ski et al., 1967; Kazenas et al., 1974). (Reaction 5a is the dominant one). Nevertheless, we believe that data of fair reliability can be obtained over a limited temperature range. This is valuable as there is but one previous attempt at a direct determination of the free energy of formation of OsO_2 in the literature (Franco and Kleykamp, 1972: the reported precision of which was only ± 3.8 kJ/mol). Studies on the thermochemical properties of two of the three other lowest valence-state PGE oxides, PdO and Rh_2O_3, using the same experimental methods as used in this work, have been presented elsewhere (Nell and O'Neill, 1996, 1997).

2. EXPERIMENTAL MEASUREMENTS

2.1. Electrochemical Measurements

High temperature electrochemical cells of the type:

$$\text{Pt, } LaCrO_3,\ M + MO_2 | \text{CSZ} | \text{YDT/air, Pt} \quad (6)$$

where M = Ru, Os, or Ir were constructed as described in O'Neill (1988; see Fig. 1 in that paper), but using the dimensions detailed in O'Neill and Pownceby (1993). YDT refers to yttria-doped thoria, which becomes a nonstoichiometric p-type semiconductor at high oxygen fugacities such as that of air, and which thus acts as a reservoir for oxygen at the reference electrode. The $LaCrO_3$ disc protects the sample electrode from reaction with the Pt lead wire.

To minimize the temperature gradient across the working part of the cell, two identical $Pt/Pt_{90}Rh_{10}$ (type S) thermocouples were used in the construction of the cell, one positioned just above the sample,

the other just below the YDT/air reference electrode. The position of the entire cell could be adjusted up or down until both thermocouples read the same (or in practice, nearly the same, with empirical corrections for small (<1 K) temperature gradients made as described in O'Neill, 1988). Temperatures are reported using the ITS 90 temperature scale. All thermocouples were calibrated individually against the melting point of Au, and the emf of each thermocouple was then corrected assuming a constant correction factor. The correction factors were within the range 1.0008 to 1.0015. The same bottom (air reference) thermocouple was used for the entire series of experiments reported here, and was calibrated both before and afterwards. The apparent drift was 0.3 K, which is approximately the uncertainty to which we believe the reported temperatures are accurate. The reference pressure used in this study is 1 bar (10^5 Pa), uncertainties are reported as ± 1 standard deviation, and the subscript 298K is to be understood as referring to 298.15 K.

We studied two Ir + IrO_2 cells, one with a relatively low ratio of Ir to IrO_2, mainly concentrating on the low temperature end at which data could be obtained (cell Ir#1); the other, with a higher ratio of IrO_2 to Ir, at the high temperature end (Ir#2). Studying electrodes with different IrO_2/Ir ratios was thought to be tactically desirable because of the relatively large amount of reaction (i.e., decomposition/formation) of IrO_2 which is needed to equilibrate with gas with a partial pressure of ~ 1 bar of O_2 near the high temperature limit of our study. For the Ru + RuO_2 and Os + OsO_2 equilibria, one cell of each type was studied.

2.2. Starting Materials

The sample electrode pellets were prepared from Ru powder (Strem Chemicals, Inc., 99.95%, −325 mesh) and RuO_2 (Strem), Ir black and IrO_2 (both Heraeus), and Os (Heraeus, 99.9%, <60 μm) and OsO_4 (Strem). For the Ru and Ir experiments, the sample electrode pellets were pressed from the metals and oxides, mixed thoroughly under acetone, in the form supplied by the manufacturors, i.e., without further treatment. We used 1 g metal and 1 g RuO_2 or IrO_2 for runs Ru#1 and Ir#1, and 1 g metal and 1.5 g IrO_2 for Ir#2. There is evidence (e.g., Mattioli and Wood, 1988; O'Neill and Pownceby, 1993) that oxides with poor crystallinity or excessively fine-grain size, which consequently possess metastably high free energies, have given erroneous results in electrochemical experiments. Here, however, we avoided attempting to recrystallize RuO_2 or IrO_2 at high temperatures because of their volatility under oxidizing conditions. Despite this, it is unlikely that the initially poor crystallinity of the oxides posed an experimental problem, as the oxides recrystallize readily during the course of the measurements. The exception is the IrO_2 in run Ir#1, which was not heated above 1190 K, and for which the subsequent XRD examination revealed some broadening of the diffraction peaks. However, the results from this run are in good agreement with those from the second Ir cell (Ir#2), in which, as in all other samples, both metal and oxide phases gave powder XRD patterns with extremely sharp peaks.

The Os + OsO_2 sample electrode was prepared from a mixture of Os metal and OsO_4 crystals, as we were unable to locate a commercial supplier of OsO_2. A mixture of 1g Os metal and 0.8 g OsO_4 was lightly ground together without any solvent, and the mixture placed into a CSZ crucible of a size which fitted neatly into the bottom of the CSZ sample tube designated for use in the subsequent Os experiment. This was sealed in the usual manner, and placed in the vertical tube furnace as for a normal emf experiment. The arrangement was then heated slowly to 200°C (i.e., well above the melting point of OsO_4 at ~40°C), at which temperature it was left for 16 hours. The temperature was then increased slowly over a period of several hours to ~700°C, left for 9 days, before cooling to room temperature by turning off the power. The reacted material was retrieved from the CSZ tube, and 1.4 g of it mixed with a further 0.4 g Os metal, which was pressed into a pellet and loaded in the usual way.

2.3. Differential Scanning Calorimetry

The heat capacities at constant pressure (C_p) of RuO_2 and IrO_2 were measured in the temperature range 370 to 1070 K with a Seteram PC 92 differential scanning calorimeter. This calorimeter consists of a silver block with two horizontal cylindrical holes bored through it and lined with alumina tubing, and surrounded by thermopiles. The calorimeter measures the differential heat flow, which occurs following an increase in temperature of the block, between a "reference" and a "sample" which are placed more-or-less symmetrically in two near-identical capsules in the centre of each of the two boreholes. The operation of the calorimeter is computer-controlled, using software provided by Seteram. The measurement routine used in this study is described in Nell and O'Neill (1996), and was developed to maximize accuracy, given the capabilities of the calorimeter. Briefly, the calorimeter was used in the step-scanning mode, in which the temperature of the calorimeter is increased in steps of 4.0 K at a rate of 1.0 K per minute, and then allowed to equilibrate thermally for 10 min before the next 4.0 K step. The measurements were made relative to α-Al_2O_3, as follows. The samples and the α-Al_2O_3 were contained in Pt capsules with tight-fitting lids, provided by Seteram. Firstly, a "blank" or "baseline" run was made, in which the two capsules, one arbitrarily designated the "sample" capsule and the other the "reference" capsule, were filled with approximately equal amounts of α-Al_2O_3. On the completion of this run the α-Al_2O_3 was emptied out of the "sample" capsule, which was refilled with the actual sample material (i.e., RuO_2 or IrO_2). The amount of sample material was chosen such that its total heat content, as calculated from its estimated heat capacity, was slightly greater than the heat content of the α-Al_2O_3 which had been emptied from the "sample" capsule. The calorimeter was then rerun under the identical step-heating program to the initial "blank" run. The heat capacity of the sample at each step is given by the measured heat flow (which by design is close to but slightly greater than zero and thus subject to minimum systematic error) plus the heat capacity of the α-Al_2O_3 previously emptied out of the capsule (which was taken from the literature; Robie et al., 1978). Measurements for both RuO_2 and IrO_2 were made in duplicate, after which the "sample" capsule was again filled with α-Al_2O_3 and a second "blank" run made. This generates four permutations of "sample" with "blank" runs for each substance, which were averaged. The precision of the method can be judged from the standard deviations of these four permutations and is approximately 0.5%, 1 standard deviation. Because of the way the measurements were made, systematic errors are kept to an minimum; quantitatively, the main source of systematic error is the heat capacity of α-Al_2O_3, which is ~0.1%. This is negligible compared to the precision of the measurements, and hence the accuracy is also taken to be 0.5%, 1 standard deviation.

2.4. Sample Characterization by Powder XRD

A small amount of material from each of the EMF sample pellets and from the DSC runs was examined after the run by powder XRD, using a STOE STADIP diffractometer in the transmission mode, typically scanning from 30 to 130° 2θ. The lattice parameters of Ru, Os, and Ir metals were also measured, using the Ru and Os starting material and some Ir from Heraeus (99.9%, <60 μ). NBS Si was used as an internal standard, except for the accurate determination of the Ir metal lattice parameter, for which the overlap of Ir with Si necessitated the use of Ge as an internal standard (a_o(Ir) = $\sqrt{2}a_o$(Si) almost exactly). This same overlap problem may cause a slight degradation in the accuracy of the results from the Ir + IrO_2 emf pellets. Peak positions were determined using whole-profile fitting methods with STOE proprietary software. Results are presented in Table 2, along with representative values from the literature.

All but one of the samples examined produced XRD patterns with sharp peaks, indicating well-crystallized material and minimal strain-broadening in the metals. The exception was the IrO_2 from the emf run Ir#1, whose peaks were noticeably broader and exhibited some asymmetry towards higher 2θ angles. This run was only heated to 1190 K, evidently insufficient to recrystallize the fine-grained IrO_2 starting material. The peak broadening and asymmetry are reflected in the lower accuracy of the lattice constants (Table 2). The Ir metal from Ir#2 gave an anomalous result, perhaps because of the Si peak overlap problem. RuO_2, OsO_2, and IrO_2 all have the undistorted rutile structure (i.e., tetragonal symmetry, space group $P4_2/mnm$).

Table 2. Lattice parameters and molar volumes at 298 K from powder XRD measurements. Some literature values are also listed (reference in parentheses).

	Metal			Oxide		
Sample (or reference)	a_o (Å)	c_o (Å)	V (cm^3)	a_o (Å)	c_o (Å)	V (cm^3)
Ru#1	2.7059(2)	4.2817(3)	8.175(1)	4.4909(2)	3.1065(2)	18.865(2)
DSC				4.4917(1)	3.1064(1)	18.871(1)
Ru (Strem)	2.7060(1)	4.2822(1)	8.177(1)			
(Schröder et al., 1972)	2.7055	4.2832	8.176			
(Rao & Iyengar, 1969a)				4.4909(3)	3.1064(4)	18.865(4)
(Rogers et al., 1969)				4.4906(2)	3.1064(2)	18.862(2)
Ir#1	3.8406(4)		8.529(3)	4.5013(14)	3.1558(18)	19.253(16)
Ir#2	3.8424(2)[a]			4.4992(2)	3.1538(2)	19.223(2)
DSC				4.4988(1)	3.1549(1)	19.223(1)
Ir (Heraeus)[b]	3.8398(1)[c]	8.523(1)				
(Singh, 1968)	3.8389		8.518			
(Schröder et al., 1972)	3.8387		8.516			
(Rogers et al., 1969)				4.4990(2)	3.1546(2)	19.226(2)
(Rao & Iyengar, 1969b)				4.4985(1)	3.1548(1)	19.223(1)
Os#1	2.7344(1)	4.3198(1)	8.423(1)	4.4964(8)	3.2008(10)	19.485(9)
Os (Heraeus)	2.7345(1)	4.3200(1)	8.423(1)			
(Schröder et al., 1972)	2.7349	4.3194	8.425			
(Rogers et al., 1969)				4.4968(2)	3.1820(2)	19.374(2)

[a] Dubious result—thought not to be accurate.
[b] Heraeus 99.9%, <60 μ.
[c] Using high purity Ge (a_o = 5.6576 Å) as the internal standard.

Single-crystal XRD studies of RuO_2 and OsO_2 are reported by Boman (1970a,b).

Some literature values of the lattice parameters for these oxides differ considerably from our measured values. Such discrepancies might perhaps be a manifestation of variable stoichiometry, as, for example, is seen in the isomorphous compound TiO_2 (rutile, sensu stricto) itself at low oxygen fugacities (e.g., Zador, 1967). The oxides from the emf samples of this study, being in equilibrium with their respective metals, are obviously at the low oxygen fugacity limit of their stability field at a given temperature, and might therefore be oxygen deficient. However, the molar volumes of IrO_2 and RuO_2 in these samples are identical to those from the DSC measurements. Secondly, the compositions of the RuO_2, IrO_2, and OsO_2 synthesised by Rogers et al. (1969), and the RuO_2 by Fletcher et al. (1968), were checked by gravimetric analysis and found to be stoichiometric within analytical uncertainty. Hence, the agreement between our XRD results and theirs (except perhaps for OsO_2, for which the agreement is less than perfect) suggests that our samples were also close to stoichiometric (i.e., x is probably less than 0.02 in the formula MO_{2-x}). Nor have we been able to identify any systematic trends amongst the variations in the other data, of the sort that would support the notion that some of the variation could be explained by nonstoichiometry. We therefore assume that the oxides in this study are stoichiometric.

3. CALORIMETRIC DATA: STANDARD ENTROPIES AT 298.15 K AND HIGH-TEMPERATURE HEAT CAPACITIES

3.1. Heat Capacities and Selected Entropies of RuO_2 and IrO_2

The heat capacities of RuO_2 and IrO_2 measured in this study are depicted in Fig. 1a,b. Both sets of data contained a "glitch" at ~450 K, which appears to be an artefact, perhaps caused by electronic noise. The few data in this "glitch" were removed from further consideration. Apart from this, the data join smoothly with the low-temperature adiabatic measurements of Cordfunke et al. (1989) and Burriel et al., (1987), respectively (Figs. 1a,b). They also agree well with the high-temperature heat content measurements of Cordfunke et al. (1989) and Fredrickson and Chasonov (1972) for RuO_2, and with Cordfunke (1981) for IrO_2. Consequently we made use of all these data (summarized in Table 3) in deriving, by weighted least-squares regression, a heat capacity equation for RuO_2 and IrO_2.

The data were fitted to an extended Maier-Kelley equation of the form:

$$C_p = C_p = a + bT + cT^{-2} + dT^{-0.5} + eT^2 \qquad (7)$$

It was found that the e term (in T^2) was redundant in obtaining a good fit to the data and was not used. For each substance, all the available data (i.e., both heat capacities and heat contents), listed in Table 3, were fitted simultaneously, using relative weights also listed Table 3. These relative weights were estimated from the internal precision of each set of measurements. Reported temperatures were corrected to ITS-90. In both cases satisfactory fits were obtained, with reduced chi-squared values of 1.53 and 1.30 for the RuO_2 and IrO_2 regressions, respectively.

The heat capacity and heat content measurements (both ours and in the literature) extend only to <1200 K, whereas we wish to use these heat capacity expressions to much higher temperatures (e.g., >1800 K for RuO_2). Extrapolation of the extended Maier-Kelley equation beyond the temperature range of the data used to obtain it frequently leads to problems. Although this is often due to the term in T^2, which is not used here, it is advisable to check carefully the values returned by the equation on extrapolation. In the present instance, we found that the C_p values calculated from

Table 3. Heat capacity and heat content data for RuO_2 and IrO_2.

Reference	Method	Temperature range (K)	Number of data used in fitting	Weight (%)
RuO_2				
This study	DSC	370–1065	175	0.5
Cordfunke et al. (1989)	Adiabatic	6–341	13*	0.25
Cordfunke et al. (1989)	Drop	410–757	27	0.3
Fredrickson & Chasonov (1972)	Drop	619–1175	13	0.3
IrO_2				
This study	DSC	370–1067	175	0.8
Burriel et al. (1987)	Adiabatic	6–346	12*	0.25
Cordfunke (1981)	Drop	416–937	10	0.3

* Only data above 250 K were used in the fitting.

our initial fit to the RuO_2 data decreased with increasing temperature above 1600 K, which is physically not very likely. Hence, we re-fit the data including a dummy point (a procedure advocated by Holland, 1981) of 96 J/K mol^{-1} at 1800 K, based on the shape of the C_p vs. T curve for TiO_2 (rutile) at equivalent temperatures. Inclusion of the dummy point hardly affects the quality of the fit of the remaining data (the reduced chi-squared for the fit increases from 1.53 to 1.55; this is itself an indication of the uselessness of the extended Maier-Kelley equation for extrapolation). For IrO_2, the equation as initially obtained was well behaved on extrapolation without any artificial assistance. The heat capacity equations are given in Table 4, and are compared to the C_p data in Fig. 1.

The entropies at 298.15 K (S°_{298K}) of RuO_2 and IrO_2 have been determined by Cordfunke et al. (1989) and Burriel et al. (1987), respectively, and these values, which probably have an uncertainty of <0.2% (e.g., Cordfunke et al., 1989), have been adopted (Table 4).

3.2. Calorimetric Data for Ruthenium, Iridium, and Osmium Metals

The calorimetric data for Ru, Ir, and Os metals needed for the third-law analyses of our EMF measurements are listed in Table 4, and were selected as follows.

The low-temperature heat capacities of the platinum group metals, including Ru and Ir, were reviewed by Furakawa et al. (1974), and values of S°_{298K} recommended. The values of S°_{298K} for Ru and Ir were mainly based on the measurements of Clusius and Piesbergen (1959) and Clusius and Losa (1955) respectively. Insufficient data existed for Furakawa et al. (1974) to evaluate S°_{198K} for Os. Subsequently, S°_{298K} for Ru has been redetermined by Naumov et al. (1991), with good agreement with the earlier value (28.50 ± 0.07 J K^{-1}mol^{-1} as compared to 28.61 from the evaluation of Furukawa et al., 1974). Naumov et al. (1988) have also determined S°_{298K} for Os. The value of S°_{298K} for Ir has not been redetermined in recent times. But in view of the evident reliability of the work of Clusius and co-workers demonstrated by the concordance of their Ru data with the later study of Naumov et al. (1991), there is no reason to suspect that the value assessed in Furakawa et al. (1974) is much in error.

High-temperature heat content data for the platinum group metals have recently been reviewed by Arblaster (1995a,b, and c), whose compilations we have used as a guide to the literature. We have refitted the selected data to our preferred form of the heat capacity equation (Eqn. 7), with weighting as described below. Temperatures were corrected to ITS-90.

Earlier compilations of thermodynamic data for Ru, Ir, and Os have all, in effect, relied on the heat content measurements of Jaeger and Rosenbohm (1932) for the high temperature heat capacities. More recently, heat contents for Ru have been measured by Cordfunke and Konings (1989) at 469 to 879 K, and by Ramanauskas et al. (1988) from 1101 to 2580 K. These two sets of measurements appear to be in good agreement with each other, but are 3 to 4% higher than the Jaeger and Rosenbohm (1932) measurements. The older study was therefore assumed to be in error and our heat capacity equation was obtained by simultaneously fitting the adiabatic heat capacity measurements of Naumov et al. (1991) in the range 253 to 311 K (10 data, assumed weight 0.1%), the 15 heat content data of Cordfunke and Konings

Table 4. Calorimetric data. High temperature heat capacity equations are from data assessed in this study (see text), except for O_2.

Phase	$S^\circ_{298.15K}$ (J K^{-1} mol^{-1})	$C_p = a + bT + cT^{-2} + dT^{-0.5}$ (J K^{-1} mol^{-1}) a	b ($\times 10^3$)	c ($\times 10^{-5}$)	d
O_2	205.15[1]	47.255	−0.455	4.402	−393.5
Ru	28.50[2]	13.054	10.052	−3.457	205.2
Os	32.55[3]	10.001	7.582	−5.722	330.5
Ir	35.48[4]	20.498	6.932	−1.227	67.4
RuO_2	46.15[5]	119.277	0.626	−1.058	−1074.6[6]
OsO_2		(88.237	6.094	−7.664	−445.5)[7]
IrO_2	50.99[8]	87.603	6.206	−7.799	−432.7

[1] JANAF tables (Chase et al., 1985). C_p data corrected to ITS90.
[2] Naumov et al. (1991).
[3] Naumov et al. (1988).
[4] From the assessment of Furakawa et al. (1974).
[5] Cordfunke et al. (1989).
[6] Fit includes a dummy point at 1800 K (C_p = 96.0 J K^{-1} mol^{-1}), see text.
[7] Estimated assuming $C_p(OsO_2) = 0.98\ C_p(IrO_2) + 0.02\ C_p(RuO_2)$.
[8] Burriel et al. (1987).

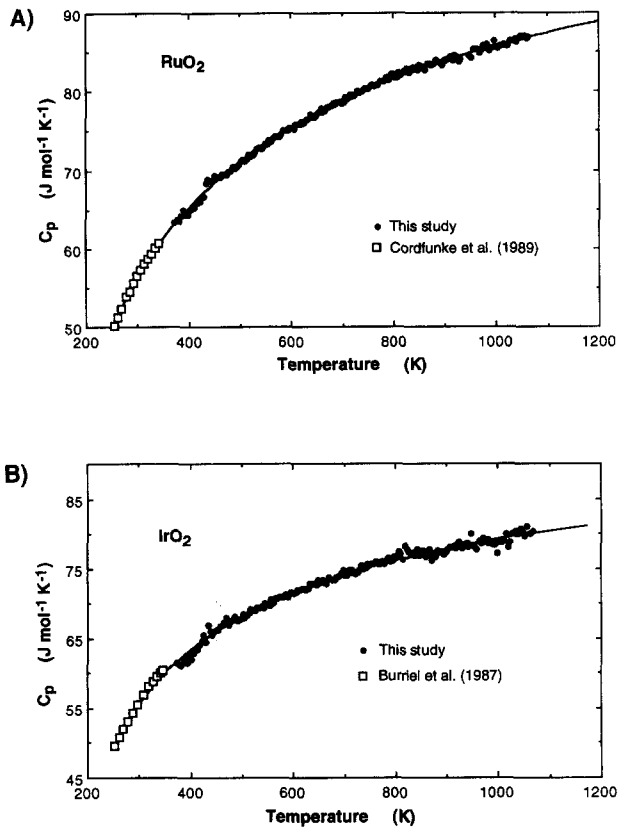

Fig. 1. Heat capacities at constant pressure (C_p) at 1 bar for (a) RuO_2 and (b) IrO_2 with the least squares best fit to these data combined with the heat content data, listed in Table 3.

(1989) with a weight of 0.3%, and the heat content data of Ramanauskas et al. (1988) up to 2200 K (40 data, assumed weight 0.3%). The equation fits the data well within these assumed uncertainties (the reduced chi-square for the regression was 1.49).

For Ir, the heat contents of Jaeger and Rosenbohm (1932) are lower than those of Ramanauskas et al. (1987) by ~1.5% in the temperature range where they overlap. We have preferred the latter workers' measurements because of the consistency of their Ru data with those of Cordfunke and Konings (1989). Our heat capacity equation was obtained by regression of the smoothed heat capacity values tabulated in Furukawa et al. (1974) between 260 and 300 K (5 data, assumed weight 0.1%) and the 14 heat content data of Ramanauskas between 1121 and 2194 K, with a weight of 0.3%. The reduced chi-square for the regression is 1.11. The equation is thus an excellent fit to precise and apparently accurate data, but it should be remembered that there is a large hole in the data coverage between 300 and 1100 K, and accordingly the shape of the heat capacity curve is poorly constrained in this region.

Our treatment of the Os data was similar to that for the Ir data. The heat contents of Jaeger and Rosenbohm (1932) for Os are also lower than those of Ramanauskas et al. (1987), by ~1.5%. So we again selected the latter measurements and combined the 24 data between 1153 and 2195 K with an assumed weight of 0.5% with the 14 heat capacity data of Naumov et al. (1988) in the range 254 to 316 K. The latter show an unusually high degree of scatter for low-temperature adiabatic heat capacity measurements (not apparent in the data below 250 K). From the observed scatter, a weight of 0.6% was assumed appropriate, and with this weight, the reduced chi-square is 1.06. As for Ir, there is a conspicuous hole in the data coverage from 300 to 1100 K.

4. RESULTS FROM THE ELECTROCHEMICAL CELLS

4.1. Performance of the Cells: Some General Considerations

Sluggish reaction kinetics of the sample electrode, rather than anything to do with the properties of the CSZ electrolyte (or any other part of the cell), is usually the factor setting the low temperature limit at which accurate data can be obtained with the electrochemical method used in this study. The empirical low temperature limit found here of about 900 to 950 K for all three equilibria is similar to the limits previously observed for the other two phase metal-metal oxide equilibria involving dioxides with rutile-like structures (i.e., Mo + MoO_2, O'Neill, 1986; W + WO_2, O'Neill and Pownceby, 1993; and Re + ReO_2, Pownceby and O'Neill, 1994). This low-temperature limit is distinctly higher than that found for other simple metal-metal oxide equilibria, which have been measured down to ~750 K in similar cells (e.g., for equilibria involving Fe, Ni, Co, Cu, or Pd; O'Neill and Pownceby, 1993: Nell and O'Neill, 1996). Bannister (1984) was able to obtain high quality data down to 645 K for the Pb + PbO equilibrium, presumably due to Pb metal being liquid.

In contrast with the low temperature limit, the high temperature ceiling of our experimental arrangement is often set by the properties of the CSZ electrolyte itself. The reason for this is well understood. CSZ works as an ideal solid-state electrolyte because the ionic component of its electrical conductivity (σ_{ion}) greatly exceeds the electronic component (σ_{el}); σ_{el}, however, need not be completely zero (Nernstian behaviour is expected when $\sigma_{ion} > 100\ \sigma_{el}$; see, e.g., the review of primary references in O'Neill and Pownceby, 1993). With increasing temperature, both σ_{ion} and σ_{el} increase according to the usual Arrhenius type of relationship until a temperature is reached at which the magnitude of σ_{el} becomes sufficient in absolute terms (but still not necessarily large relative to σ_{ion}) such that a significant amount of oxygen may be short-circuited from one electrode to the other. "A significant amount" is defined with respect to the effective buffering capacity of one or another of the electrodes, kinetic factors included (i.e., the ability of the electrode to react out the amounts of short-circuited oxygen). The short-circuiting then results in a drop in the emf of the cell. Since σ_{el} in CSZ is itself a function of μO_2, the point at which this phenomenon becomes a problem depends on the μO_2 values defined by the sample and reference electrode and the difference between them, as well as the effective buffering capacities of the two electrodes. Thus, it is difficult to assess, a priori, at what temperature a cell may begin to suffer from this problem. From a practical point of view, the identification of the problem is often best done by subsequently examining the data for any anomalous decrease of the emf com-

Table 5. Results from the cell Pt ($LaCrO_3$), Ru + RuO_2|CSZ|YD-T(air), Pt, listed in the order in which the measurements were made.

T (K)	O_2 (kJ mol^{-1})	T (K)	O_2 (kJ mol^{-1})
963.8	−139.594	1232.3	−94.385
922.2	−147.502	1129.5	−111.373
878.7	−156.690	1293.5	−84.325
900.5	−152.623	1314.0	−80.980
921.0	−147.642	1334.5	−77.655
942.9	−142.805	1354.5	−74.423
963.4	−139.331	1374.9	−71.105
985.2	−135.651	1395.0	−67.869
1006.3	−132.073	1354.2	−74.516
1026.3	−128.673	1313.8	−81.095
1046.6	−125.404	1273.0	−87.736
1067.9	−121.729	1232.7	−94.358
1088.4	−118.243	1293.6	−84.359
1108.2	−114.938	1334.5	−77.724
1129.4	−111.418	1374.8	−71.171
1150.1	−107.961	1414.9	−64.704
1108.4	−114.995	1434.7	−61.481
1067.8	−121.864	1454.8	−58.228
1026.3	−128.843	1474.4	−55.050
984.6	−135.913	1394.6	−68.006
1005.8	−132.297	1334.1	−77.784
1046.7	−125.350	1414.7	−64.731
1088.5	−118.290	1474.5	−55.070
1129.5	−111.409	1494.8	−51.761
1170.4	−104.586	1514.6	−48.550
1191.5	−101.099	1534.5	−45.284
1212.0	−97.708	1553.8	−42.090
1232.2	−94.396	1573.6	−38.872
1150.4	−107.919	1593.1	−35.664
1150.7	−107.839	1612.6	−32.476
1252.6	−90.986	1494.4	−51.739
1273.0	−87.652	1374.2	−71.052

pared with trends established from lower temperatures. This is conveniently done by graphical inspection of the results of the third-law analysis of the data.

4.2. Ru + RuO_2

The electrochemical experiment was brought to the initial temperature (964 K) and left for 71 hours to equilibrate. Thereafter data were obtained at intervals of 40 min to 2 days, depending on temperature. The total run time was 22 days.

The data are given in Table 5 in the order in which they were obtained. The third law analysis of these data, using the calorimetric data of Table 4, is shown in Fig. 2. It is apparent that the four lowest temperature data (879 to 922 K) trend anomalously to lower (more negative) values of μO_2. This deviation is in the opposite sense and is also much more pronounced than that observed for the Ir + IrO_2 and Os + OsO_2 equilibria at low temperatures (see below), and also for W + WO_2 below ~ 940 K (O'Neill and Pownceby, 1993). A possible explanation for this is that the Ru + RuO_2 equilibrium intersects an equilibrium involving another Ru oxide below ~930 K (e.g., if the hypothetical compound Ru_2O_3 were stable at low temperatures). To explore this possibility, a sample of Ru plus RuO_2 was intimately mixed together and sintered in an evacuated silica tube at 600°C for 65 days. However, powder XRD showed only Ru metal and RuO_2 as in the starting material. This negative result does not definitively preclude the existence of another Ru oxide at low temperatures, since the extent of any reaction may be too small to detect. However, other workers have not found similar anomalous behaviour even at temperatures as low as 750 K (e.g., Pizzini and Rossi, 1971; Mallika and Sreedharan, 1990), and we tentatively conclude that our results below 930 K simply reflect a failure of our Ru + RuO_2 electrode to maintain equilibrium. In any event, these four anomalous data were excluded from further consideration.

At high temperatures, we were able to obtain data up to 1611 K without observing the decrease of emf expected from the electronic short-circuiting of the cell discussed above. Although the third-law analysis suggests that the five highest temperature data above 1515 K are in fact probably slightly affected by such short-circuiting (see Fig. 2), to obtain accurate data even to 1515 K is, by comparison with what is normally achievable with our experimental design, a noteworthy feat. Four factors may contribute to this success: (1) the optimum μO_2 for CSZ electrolytes is relatively high and is probably approximately in the vicinity of air and the Ru + RuO_2 buffer, (2) the μO_2 of Ru + RuO_2 converges towards that of the reference electrode (air) at high temperatures anyway (the intersection is at 1683 K), (3) neither Ru nor RuO_2 react chemically with other components in the cell, and (4) the Ru + RuO_2 electrode does not seem to sinter down to lower porosities in the temperature range of the experiments, and therefore maintains a fairly high surface area with which to equilibrate with the Ar-rich atmosphere above the electrode.

For the remaining data, 55 measurements between 934 and 1515 K, the calculated values of $\Delta_f H^\circ_{298.15K}$ show a small decrease with temperature, indicating some discrepancy with the calorimetric data for Ru or RuO_2, or both. Regression of the calculated values of $\Delta_f H^\circ_{298.15K}$ gives:

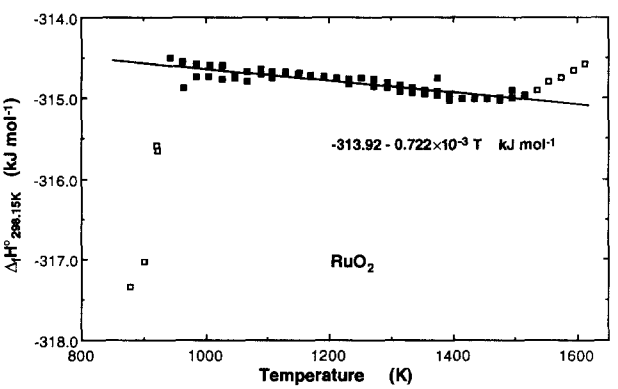

Fig. 2. Values of $\Delta_f H^\circ_{298}$ for RuO_2 calculated from the third-law analysis of the emf data (Table 4), using the calorimetric data summarized in Table 3, plotted against the temperature of the datum. Perfect agreement between the emf measurements and the calorimetric data would result in calculated values of $\Delta_f H^\circ_{298}$ which were independent of temperature, i.e., a horizontal array. The slightly negative slope of −0.722 J K^{-1} mol^{-1} indicated by the best fit line indicates a discrepancy with the calorimetric data of this magnitude. Data plotted as open symbols are thought to be subject to systematic error, and were not used in deriving the best fit line.

$$\Delta_f H^\circ_{298.15K}\ (\pm 71) = -313918(\pm 72) - 0.7221(\pm 0.0584)\ T \quad \text{J mol}^{-1} \quad (8)$$

Although at one level the present results may be considered to be in fairly good agreement with these calorimetric data in that the discrepancy is only 0.7 J K^{-1} mol^{-1}, this is still greater than the assessed uncertainties in the calorimetrically determined entropy of the reaction at 298.15 K, which are only ~0.2 J K^{-1} mol^{-1}. However, this does not include possible contributions from the uncertainties in the high temperature Cp data, which cannot be precisely evaluated. It is debatable in this kind of situation whether the calorimetric data should be treated as being perfectly accurate and an average value of $\Delta_f H^\circ_{298K}$ selected (i.e., $\Delta_f H^\circ_{298K}$ would -314.80 ± 0.14 kJ mol^{-1}), thus implying a temperature-dependent systematic error of unknown origin in our emf experiments, or if the nonconstant nature of $\Delta_f H^\circ_{298.15K}$ should be accepted as real, implying error in the calorimetrically determined entropies and heat capacities. Since in order to produce a summary of the thermodynamic data of RuO_2 we must take a position on this issue, we somewhat arbitrarily choose the latter option, as we have no reason to believe that our experimental method should produce systematic errors as a function of temperature. (It is only fair to add that we have no reason to suspect the calorimetric data either; hence, the impasse.) To resolve the matter with a new calorimetric determination of $\Delta_f H^\circ_{298.15K}$ would require such a measurement to be done with extreme accuracy.

The expression for $\Delta_f H^\circ_{298K}$ in Eqn. 8 was recombined with the calorimetric data to obtain a smoothed expression for the μO_2 of the Ru + RuO_2 equilibrium (equivalent to the free energy of formation, $\Delta_f G^\circ_T$, of RuO_2, with the assumption that RuO_2 is stoichiometric and Ru metal is pure, i.e contains no oxygen):

$$Ru + RuO_2\text{: } \mu O_2 = -324563 + 344.151\ T - 22.1155\ T \ln T \quad \text{J mol}^{-1} \quad (9)$$

which is valid from 700 to 1800 K. This procedure makes use of the heat capacity data to constrain as well as possible the curvature of the μO_2-T relationship. While the observed standard deviation of the experimental data from this equation is only ±71 J/mol, this is a measure only of the scatter in the data and does not include possible systematic errors; experience with duplicate experiments (see O'Neill and Pownceby, 1993) indicates that a more realistic uncertainty is probably about ±200 J/mol.

The heat of formation of RuO_2 was measured by Shchukarev and Ryabov (1960) by combustion calorimetry. They obtained a value of −305.2 kJ/mol, but with a standard deviation of ±6.2 kJ/mol. The present results are thus not inconsistent with this rather imprecise measurement, within an uncertainty of two standard deviations.

4.3. Ir + IrO_2

Two Ir + IrO_2 cells were studied, the first (Ir#1, with Ir:IrO_2 1:1 by weight) in the temperature range 963 to 1171 K, the second (Ir#2, Ir:IrO_2 1.5:1 by weight) from 879 to 1414 K. Ir#1 was initially heated at 1089 K for 50 hours, and then readings taken at intervals of 2 to 16 hours, depending on temperature. The total run time was 11 days. Run Ir#2 was initially heated to 964 K for 44 hours, readings obtained at intervals from 40 min to 48 hours, with a total run time of 20 days. The results from the two runs are given in Table 6, and the third-law analysis is presented in Fig. 3. There is good agreement between the results from the two cells. In addition to demonstrating the thermal reversibility of the cells, we checked for equilibrium at 1293 K in run Ir#2 by evacuating the gas above the Ir + IrO_2 sample electrode and refilling with pure O_2. Following this procedure the emf returned close to its previous value at the same temperature within 6 hours.

The high temperature limit to which the cell Ir#2 was taken was 1414 K, at which temperature the μO_2 corresponds to an oxygen pressure of 1.6 bars. Our cells are not designed for pressures inside the sample electrode compartment substantially greater than atmospheric pressure, and higher pressures could have resulted in a blow-out of the epoxy seals, allowing air into the sample electrode. Were the experiment to have failed in this manner, it would not have been possible to have checked the thermal reversibility of the cell by taking measurements at lower temperatures, and oxidation by the

Table 6. Results from the cells Pt ($LaCrO_3$), Ir + IrO_2|CSZ|YDT(air), Pt, listed in the order in which the measurements were made.

T (K)	μO_2 (kJ mol^{-1})	T (K)	μO_2 (kJ mol^{-1})
Cell Ir#1		901.0	−82.841
1088.7	−50.205	922.5	−79.313
1067.9	−53.902	943.5	−75.749
1047.1	−57.621	963.8	−72.157
1026.4	−61.296	985.8	−68.295
1006.1	−64.949	1006.1	−64.813
984.8	−68.729	1026.3	−61.217
963.0	−72.623	1046.9	−57.589
984.9	−68.768	1067.7	−53.869
1006.1	−65.000	1088.7	−50.267
1026.4	−61.369	1108.2	−47.244
1046.9	−57.701	1129.4	−43.108
1068.0	−53.950	1149.8	−39.657
1088.7	−50.317	1170.3	−36.182
1108.4	−46.814	1191.2	−32.529
1129.6	−43.086	1211.9	−28.956
1150.1	−39.474	1232.1	−25.468
1170.5	−35.980	1253.0	−21.975
1129.6	−43.238	1252.4	−22.115
1088.7	−50.419	1272.6	−18.633
1046.7	−57.891	1293.0	−15.103
1006.0	−65.128	1313.3	−11.577
962.8	−72.738	1272.6	−18.707
984.9	−68.919	1231.8	−25.773
1026.4	−61.524	1191.4	−32.837
1067.8	−54.186	1292.9	−15.209
1108.4	−47.008	1292.9[1]	−15.288
1149.9	−39.619	1333.8	−8.214
1191.4	−32.444	1353.8	−4.772
Cell Ir#2		1374.3	−1.246
964.1	−72.042	1394.6	+2.185
943.5	−75.627	1414.6	+5.566
922.5	−79.183	1313.3[1]	−11.910
901.1	−82.863	1414.3	+5.423
879.1	−86.523		

[1] Ir + IrO_2 electrode compartment pumped out and pure O_2 added.

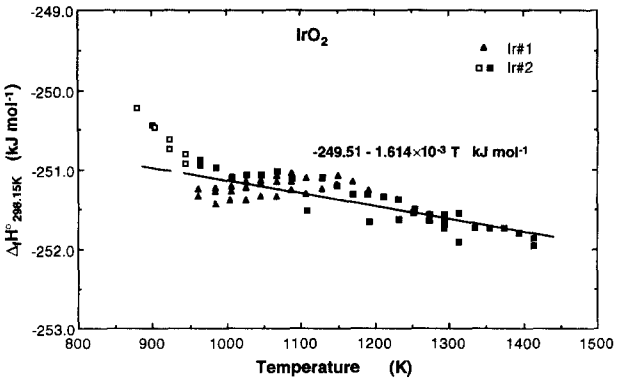

Fig. 3. Values of $\Delta_f H^\circ_{298}$ for IrO_2 calculated from the third-law analysis of the emf data. Data plotted as open symbols are thought to be subject to systematic error, and were not used in deriving the best fit line.

air would also have prevented characterisation of the Ir + IrO_2 electrode. Thus, higher temperatures were not risked, and, in this case, the high temperature limit of the measurements is set by the properties of the sample, not of the CSZ electrolyte.

The third-law analysis also shows a slight decrease of calculated $\Delta_f H^\circ_{298K}$ with increasing temperature. Ignoring the data below 950 K, which seem to trend slightly to more oxidizing values, and which therefore may not have equilibrated fully, regression of the remaining 60 data from both runs gives

$$\Delta_f H^\circ_{298K}\ (\pm 156) = -249508(180) - 1.6138(0.1568)\ T \quad \text{J mol}^{-1} \quad (10)$$

The drift relative to the calorimetric data (1.6 J K^{-1} mol^{-1}) is thus different than that found for the Ru + RuO_2 equilibrium, which can be construed as an argument against a systematic temperature-dependent error in our experimental design. Recombining this expression with the calorimetric data gives the smoothed expression

$$\text{Ir} + \text{IrO}_2\text{: } \mu O_2 = -256518 + 295.854\ T - 15.2368\ T \ln T \quad \text{J mol}^{-1} \quad (11)$$

which should be valid within an estimated uncertainty of ±300 J/mol between 700 and 1500 K.

4.4. Os + OsO_2

The behaviour of the cell and the results from it (Table 7 and Fig. 4) were unexceptional below ~1080 K. The cell came smoothly to a steady value of its emf at the initial temperature of 962 K within about 6 hours. The third-law analysis shows that the data below ~920 K trend towards more oxidized values (Fig. 4), indicating that the Os + OsO_2 assemblage may have failed to equilibrate fully at these temperatures. As noted above, a similar failure to equilibrate is observed in other $M + MO_2$ buffers (including Ir + IrO_2) at similar temperatures in analogous electrochemical cells. These data were excluded from the fitting procedure.

Table 7. Results from the cell Pt ($LaCrO_3$), Os + OsO_2|CSZ|YD-T(air), Pt, listed in the order in which the measurements were made.

T (K)	μO_2 (kJ mol^{-1})	T (K)	μO_2 (kJ mol^{-1})
962.4	−119.744	1046.0	−105.650
941.8	−123.237	962.7	−119.892
920.9	−126.755	984.4	−116.304
899.5	−130.171	1005.5	−112.931
876.9	−133.816	1025.8	−109.529
877.9	−133.564	1046.3	−106.072
857.2	−136.778	1067.1	−102.323
878.0	−133.634	1087.9[1]	−98.952[2]
899.9	−130.121	1107.7	−95.446[2]
921.4	−126.890	1128.7	−91.713[2]
942.3	−123.279	1149.3	−88.100[2]
962.3	−119.867	1169.4	−84.529[2]
984.1	−116.130	1190.5	−81.021[2]
1005.0	−112.643	1211.3[3]	−79.092
1025.6	−109.116	1231.5	−77.632
1046.0	−105.633	1252.3	−75.923
1067.1	−102.058	1272.6	−74.426
1087.9	−98.559	1231.9[4]	−77.335
1067.0	−102.150	984.8	−116.329

[1] The emf of the cell became unsteady (0.5 mV) after 8 hrs at this temperature.
[2] Unsteady emf (0.5 mv)[3] emf became steady again.
[4] Os + OsO_2 electrode compartment pumped out and air added.

The behaviour of the cell above ~1070 K was unusual. After ~8 hours at 1088 K the emf trace on the chart recorder became distinctly wobbly, that is, showing an irregular wavy pattern with amplitude of ±0.5 mV and period of several hours. This kind of wobbliness is sometimes encountered in cells at the low-temperature limit at which they give satisfactory results, but we have not experienced it previously on increasing temperature.

The wobbliness continued at all temperature increments up to 1211 K, at which temperature the emf became quite steady once more (i.e., to better than ±0.1 mV when monitored over several hours). The third-law analysis of these wobbly data indicates that they are in good agreement with the trend of the data as established in the temperature range

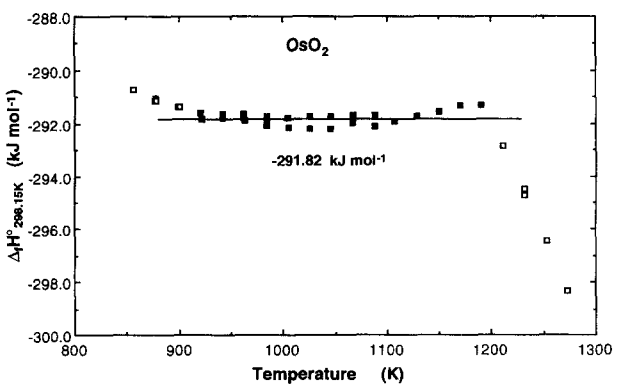

Fig. 4. Scatter of values of $\Delta_f H^\circ_{298}$ for OsO_2 calculated from the third-law analysis of the emf, using $S^\circ_{298}(OsO_2)$ = 54.8 J K^{-1} mol^{-1}, selected to give a zero slope to the array. Data plotted as open symbols are thought to be subject to systematic error, and were not used.

921 to 1067 K. Steady and apparently also thermally reversible emfs (see datum at 1232 K in Table 7 taken on decreasing temperature) were obtained in the range 1211 to 1273 K, but these results deviate sharply to more reducing conditions (Fig. 4). This is in the opposite direction to that expected if the CSZ electrolyte were developing significant electronic conductivity (cf. high temperature behaviour of the Ru + RuO_2 cell in Fig. 2). We surmise that the explanation for this behaviour is that the μO_2 of the sample electrode is no longer being set by the Os + OsO_2 assemblage, but rather by $OsO_4(g)$ and $OsO_3(g)$, produced by the disproportionation of the $OsO_2(s)$ according to reactions 5a and b, in equilibrium with Os. According to a linear extrapolation of the data of Nikol'ski et al. (1967) on the pressures of $OsO_4(g)$ and $OsO_3(g)$ in equilibrium with Os + OsO_2 (which we have attempted to recover from the tiny graph in that paper), the combined pressures of $OsO_4(g)$ and $OsO_3(g)$ would reach ~1.6 bars at 1200K, lending credence to our hypothesis that the Os-$OsO_2(s)$ was no longer controlling the μO_2 in our cell at this and higher temperatures. Since the partial pressures of $OsO_4(g)$ and $OsO_3(g)$ in the cell are not known, however, these highest temperature data give no useful results. Lowering the cell temperature to 985 K (last datum in Table 7) seems to have re-established equilibrium between Os and $OsO_2(s)$. The experiment was then terminated and the cell opened for inspection. This revealed much transport of material from the sample pellet up the CSZ electrolyte tube, which was not observed at all in the Ru and Ir cells. The inside of the CSZ tube and the outside of the alumina push rod were heavily coated with mottled bluish-purplish-black material, thick enough near the bottom to flake off. Nevertheless, XRD analysis of the sample pellet showed that abundant well-crystallized OsO_2 remained in the sample.

Since S°_{298K} for OsO_2 has not been determined calorimetrically, we are unable to test our results by the third law method. Instead, we can use Eqn. 4 combined with measured and estimated high-temperature heat capacities for Os and OsO_2 (Table 4), respectively, to derive a values of S°_{298K} and $\Delta_f H^\circ_{298K}$ for OsO_2. We obtain S°_{298K} = 54.78 ± 0.65 J K^{-1} mol^{-1}, with $\Delta_f H^\circ_{298K}$ = 291.83 ± 0.66 kJ mol^{-1} (uncertainties are one standard deviation). The smoothed expression for the chemical potential of oxygen defined by the Os + OsO_2 equilibrium is

$$\text{Os} + \text{OsO}_2\text{: } \mu\text{O}_2 = -300399 + 307.639\,T - 17.4819\,T \ln T \quad \text{J mol}^{-1} \quad (12)$$

that, apart from any systematic errors introduced by using estimated values of C_p for OsO_2 in extrapolating the data, should be valid from 700 to 1500 K with an estimated uncertainty of ±400 J mol^{-1}.

5. COMPARISON WITH PREVIOUS WORK

The present results are compared to the results of previous studies (Table 1) and with some compilations of high-temperature thermodynamic properties (Pankratz, 1982; Barin, 1989) in Figs. 5 to 7. For the Ru + RuO_2 equilibrium, our results agree with all eight previous experimental studies to within ±4 kJ/mol. In particular, our results are in extremely good agreement with the two most recent studies, those of Cordfunke and Konings (1988) and Mallika and Sreedharan (1990), as shown in Fig. 5b. The slightly different temperature dependence of the data of Cordfunke and Konings (1988) translates into a somewhat larger discrepancy with the calorimetric data, when analysed by the third-law method. A third-law analysis of their data using the calorimetric data in Table 4 gives:

$$\Delta_f H^\circ_{298K}\ (\pm 71) = -311185\ (\pm 648) - 3.4119\ (\pm 0.6419)\,T \quad \text{J mol}^{-1} \quad (13)$$

Hence, the "drift" relative to the calorimetric data is 3.4 J K^{-1} mol^{-1}, compared to 0.7 J K^{-1} mol^{-1} in this study.

Both Pizzini and Rossi (1971) and Mallika and Sreedharan (1990) report measurements down to 750 K which are in good agreement with our results above ~930 K, extrapolated to lower temperatures using Eqn. 8; there is no sign in these two studies of the difficulties we encountered

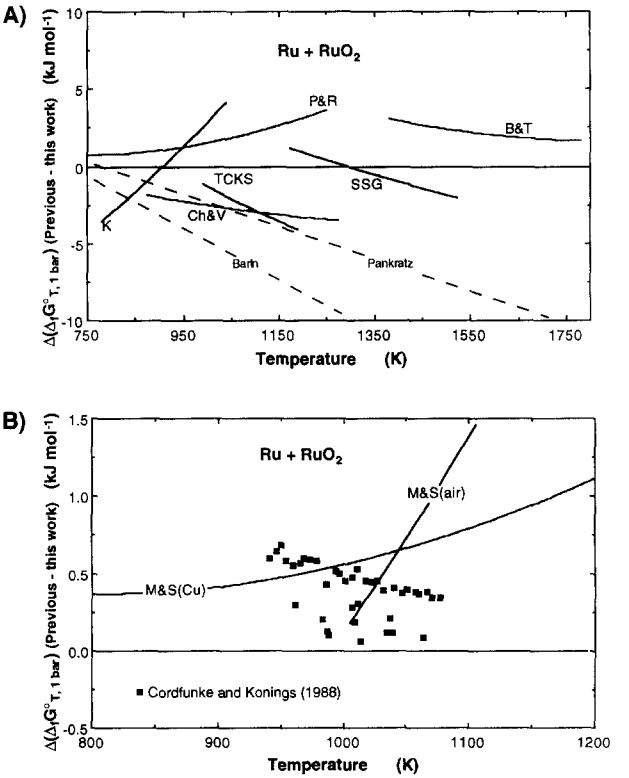

Fig. 5. (a, b) Comparison of the results of this study for $\Delta_f G^\circ_T$ of RuO_2 with previous work, as a function of the temperature at which the previous work was undertaken. Note the expanded scale of the vertical axis in Fig. 5b. Key: SSG: Schäfer et al. (1963); B&T: Bell and Tagami (1963); K: Kleykamp (1969); P&R: Pizzini and Rossi (1971); C&V: Chatterji and Vest (1971); TCKS: Tagirov et al. (1975); M&S: Mallika and Sreedharan (1990). Each datum from the study of Cordfunke and Konings (1988) which is of very good precision, is plotted individually. Also shown (dashed curves) are the values recommended by Barin (1989) and Pankratz (1982).

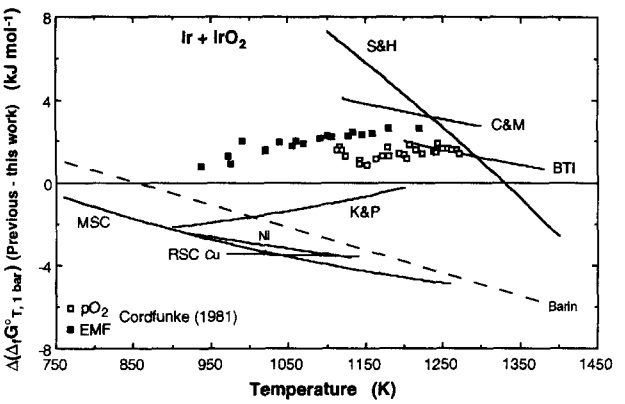

Fig. 6. Comparison of the results of this study for $\Delta_f G^\circ_T$ of IrO_2 with previous work. Key: S&H: Schäfer and Heitland (1960); C&M: Cordfunke and Meyer (1962); BTI: Bell et al. (1966); K&P: Kleykamp and Paneth (1973); RSC: Ramakrishnan et al. (1975, vs. Ni + NiO and vs. Cu + Cu_2O; MSC Mallika et al. (1985). Individual data from Cordfunke (1981) are plotted.

at lower temperatures. None of the previous EMF studies report data above 1250 K, which is curious in light of the ease with which we obtained data to >1500 K.

The values from the two thermodynamic data compilations (Pankratz, 1982, and Barin, 1989) are in poorer agreement. Both compilations use identical values for $\Delta_f H^\circ_{298K}$ (-305.0 kJ mol^{-1}, presumably from Shchukarev and Ryabov, 1960) and for S°_{298K}, for both Ru and RuO_2; thus, the difference in the two compilations at high temperatures is due to different estimates of the high-temperature heat capacities of Ru and RuO_2. The difference between these two curves illustrated in Fig. 5a is thus a useful demonstration of the importance of accurate high-temperature heat capacity data.

For Ir + IrO_2, our results are also in general agreement with most of the previous work (Fig. 6). The electrochemical study of Ramakrishnan et al. (1975) is noteworthy, as these authors report sharp changes in the slopes of their EMF vs. T curves at 920 to 970 K, similar to our observations and which we propose is due to the difficulty of achieving equilibrium with the Ir + IrO_2 electrode below ~930 K. However, Mallika et al. (1985) report no such difficulties in measurements which extend down to 762 K.

Our results for Os + OsO_2 agree well with the only previous study, that of Franco and Kleyklamp (1972) within the stated precision of the latter of ±3.8 kJ mol^{-1} (Fig. 7). The values listed in Barin (1989) are referenced as being based on the work of Franco and Kleykamp (1972).

6. SOME GEOLOGIC APPLICATIONS

6.1. Iridium and Ruthenium Solubilities in Silicate Melts and their "Magmaphobic" Behaviour

The solubility of a siderophile element in a silicate melt can be described by the reaction

$$\underset{\text{metal}}{M} + x/4\ O_2 = \underset{\text{silicate liquid}}{MO_{x/2}} \qquad (14)$$

where x is the valency of the element in the silicate melt. Referred to a standard state of the pure oxide with valence x in its solid form, at equilibrium

$$-\Delta_f G^\circ_T/RT = \ln a^{\text{sil liq}}_{MO_{x/2}} - x/4 \ln f_{O_2}$$
$$= \ln X^{\text{sil liq}}_{MO_{x/2}} + \ln \gamma^{\text{sil liq, solid s.s.}}_{MO_{x/2}} - x/4 \ln f_{O_2} \qquad (15)$$

where the activity coefficient of $MO_{x/2}$ referred to the standard state of the pure solid oxide is related to the activity coefficient of $MO_{x/2}$ referred to the pure liquid oxide by:

$$\ln \gamma^{\text{sil liq, solid s.s.}}_{MO_{x/2}} = \ln \gamma^{\text{sil liq, liquid s.s.}}_{MO_{x/2}} + \Delta G^\circ_{\text{melt}}/RT \qquad (16)$$

$\Delta G^\circ_{\text{melt}}$ is the free energy of melting of $MO_{x/2}$ (the reason for considering the two standard states is that nothing is known about the melting behaviour of any PGE oxides, as they all decompose before their melting temperature is reached). O'Neill et al. (1995) have determined the solubility of Ir in a haplobasaltic melt in the simple CMAS system (diopside-anorthite eutectic) to be 30 (±10) ppm in air (f_{O_2} = 0.20 bars) at 1400°C. This corresponds to $X^{\text{silliq}}_{IrO_2} = 8 \times 10^{-6}$, if we assume that all this Ir dissolves as Ir^{4+}. (In fact there is evidence for most PGEs that a substantial proportion of their observed solubilities in silicate melts is due to low valence species; see, e.g., O'Neill et al., 1995. Thus, the solubility of IrO_2 (i.e., Ir as Ir^{4+}) is probably even lower than indicated by the total Ir solubility, and the argument developed below will be understated.) From Eqn. 15, using the present results for $\Delta_f G^\circ_T$ extrapolated to 1400°C, we calculate that $\gamma^{\text{sil liq,solid s.s.}}_{IrO_2}$ is 2.3×10^3, which is a large number for an activity coefficient. To state the argument from another perspective: if $\gamma^{\text{sil liq,solid s.s.}}_{IrO_2}$ were unity (i.e., ideal mixing of solid IrO_2 in silicate melt), then $X^{\text{sil liq}}_{IrO_2}$ would be 0.02, and the solubility of Ir under these conditions would be ~0.1 wt%, not the ~30 ppm observed.

Similarly large activity coefficients can be deduced for Ru: Capobianco and Drake (1990) observed solubilities of 320 ± 120 and 270 ± 110 ppm Ru in CMAS melts in equilibrium with RuO_2 at 1450 and 1290°C, respectively, implying (assuming all dissolved Ru is Ru^{4+}) values of

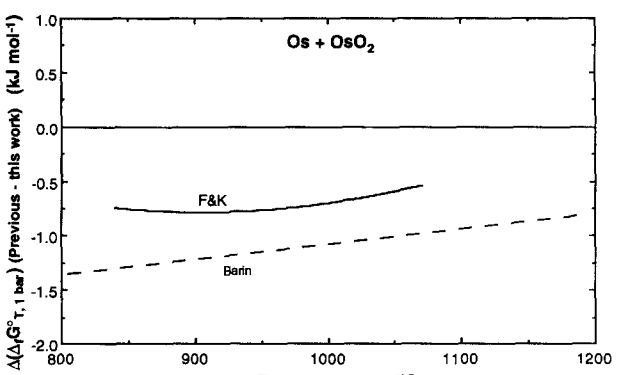

Fig. 7. Comparison of the results of this study for $\Delta_f G^\circ_T$ of OsO_2 with the only previous study in the literature, Franco and Kleykamp (1972). The values recommended by Barin (1989) are based on the Franco and Kleykamp (1972) study, but differ slightly from it for unknown reasons.

$\gamma_{RuO_2}^{\text{sil liq,solid s.s.}}$ of $\sim 1.6 \times 10^4$, even greater than the activity coefficient for IrO_2. The amount of energy implied by these activity coefficients is $RT \ln \gamma_{MO_{x/2}}^{\text{sil liq,solid s.s.}}$ i.e., about 120 kJ mol^{-1}. Other PGEs also have large activity coefficients for their oxide components in silicate melts (e.g., Pd — Nell and O'Neill, 1996), although not so extreme as those for IrO_2 and RuO_2.

One potential reason for these large activity coefficients is the use of the solid oxide standard state. If ΔG° for the PGE oxides is very large, then the values of $RT \ln \gamma_{MO_{x/2}}^{\text{sil liq,solid s.s}}$ might depend mainly on this term (Eqn. 16). However, the following argument suggests this is probably not the whole story. The entropy of melting of oxides with the MO_2 stoichiometry is ~ 30 J K^{-1} mol^{-1} (Barin, 1989: data listed for M = Ti, U, Zr, Hf, V, and Nb). Empirically an upper limit for the melting point of any substance would appear to be ~ 4000 K. This suggests that $\Delta H^\circ_{\text{melt}}$ for RuO_2 and IrO_2 would be less than ~ 120 kJ mol^{-1}, and that, therefore, at 1600 K, $\Delta G^\circ_{\text{melt}}$ would be no more than ~ 70 kJ mol^{-1}. Hence, (from Eqn. 15) $RT \ln \gamma_{MO_{x/2}}^{\text{sil liq,liquid s.s}}$ would still be >50 kJ mol^{-1}. Apparently there is something fundamental in the chemistry of the PGEs in silicate melts, apart from the (possibly) high melting points of their oxide components, which makes them "magmaphobic." Many of their important and distinguishing geochemical properties, including their extremely high metal/silicate distribution coefficients, and their apparent compatibility during mantle melting processes, derive from this unusual chemical characteristic. As regards future work, a better feel for the magnitude of $\Delta G^\circ_{\text{melt}}$ may be possible when more information is gained on the solubilities of the PGEs in silicate melts both as a function of temperature and melt composition.

6.2. Differences in Metal/Silicate and Sulfide/Silicate Partition Coefficients among the PGEs

Perhaps the most important property needed in interpreting the significance of PGE abundance patterns in mafic and ultramafic rocks is the extent to which their partitioning coefficients between silicate and sulfide (or metal) differ. Several experimental and empirical studies (e.g., Fleet et al., 1991, 1996; Peach et al., 1990, 1994; Bezmen et al. 1994) have indicated that some or even most of the PGEs have rather similar silicate-melt/sulfide partition coefficients, such that the extent of any PGE fractionation may be rather limited by sulfide segregation. However, the thermodynamic basis underlying the partioning behaviour of the PGEs suggests that this similarity in partition coefficients is not expected.

Figure 8 shows the positions of the Ru + RuO_2, Os + OsO_2, and Ir + IrO_2 equilibria in μO_2-T space, compared to some other common and geologically relevant oxygen buffers, including that for Re + ReO_2 (Pownceby and O'Neill, 1994). It can be seen that the reduction potentials of the Highly Siderophile Elements (i.e., the PGEs plus Re and Au) cover a wide range of μO_2 at constant temperature, for example, comparable to that covered by Ni and Fe. Consequently one would expect, all other things being equal, that any process involving metal/silicate or sulfide/silicate partitioning would fractionate the PGEs from each other, by

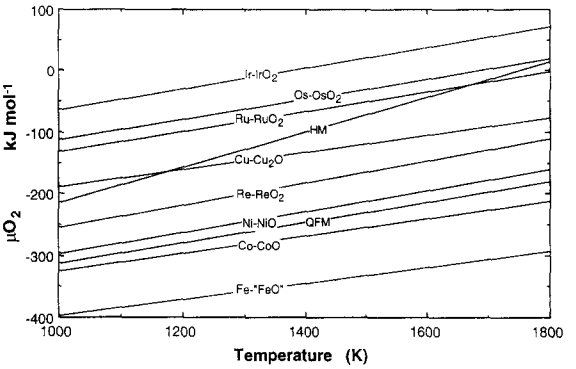

Fig. 8. Positions of the Ru + RuO_2, Os + OsO_2 and Ir + IrO_2 equilibria in μO_2-T space at 1 bar, compared to some other common oxygen buffers (QFM: 3 Fe_2SiO_4 + O_2 = 2 Fe_3O_4 + 3 SiO_2; HM; 4 "Fe_3O_4" + O_2 = 6 Fe_2O_3). Data from O'Neill (1988), O'Neill and Pownceby (1993), and Pownceby and O'Neill (1994).

considerable amounts. For Ru, Os, and Ir, this expectation can be quantified as follows.

Consider the partitioning of a PGE, M, between Fe-rich metal and silicate melt (this is for simplicity; the partitioning between the more widely studied sulfide liquid and silicate melt can be treated in identical fashion; see O'Neill et al., 1995). Equation 14 expanded to include the effect of diluting M into Fe-rich metal is

$$\ln D_M^{\text{met/sil}} = \ln k \frac{X_M^{\text{metal}}}{X_{MO_{x/2}}^{\text{sil liq}}}$$

$$= -\frac{\Delta_f G_T^\circ}{RT} + \ln \gamma_{MO_{x/2}}^{\text{sil liq,solids.s.}} - \ln \gamma_M^{\text{metal}} - \frac{x}{4} \ln f_{O_2} \quad (17)$$

Now for Ru and Ir, the values of $\gamma_{MO_{x/2}}^{\text{sil liq,sol s.s}}$ are similar (previous section) assuming $x = 4$, at least in CMAS melts. Neglecting for the sake of argument the relative values of γ_M^{metal}, the ratio of the metal silicate (or sulfide silicate) distribution coefficients for Ru and Ir should then simply be

$$D_{\text{Ir}}^{\text{met/sil}}/D_{\text{Ru}}^{\text{met/sil}} \approx \exp\{[-\Delta_f G_T^\circ(IrO_2) + \Delta_f G_T^\circ(Ru)_2)]/RT\} \quad (18)$$

i.e., about 220 at 1600 K. The same argument suggests that a similar difference in the ratios of the sulfide/silicate partition coefficients should apply. Bezmen et al. (1994) found a ratio $D_{\text{Ir}}^{\text{sulf/sil}}/D_{\text{Ru}}^{\text{sulf/sil}}$ of about this magnitude (actually 124 $\pm$ 47) in their experimental study, whereas Fleet et al. (1996) observed $D_{\text{Ir}}^{\text{sulf/sil}}/D_{\text{Ru}}^{\text{sulf/sil}} \approx 4 \pm 2$. Although our argument is an oversimplification (e.g., apart from the neglect of the activity coefficients of Ru and Ir in metal or sulfide, it is by no means certain that Ru or Ir are even dissolving in a 4+ valence state at the oxygen fugacities of the experiments), it does point towards a preference for the former result.

It is unlikely, in considering all six PGEs plus Re and Au, that such factors as the relative magnitudes of the activity coefficients or changes in valence state should happen, by chance, to combine so as to nullify the differences in the standard state properties of the highly siderophile elements,

and we believe a clear principle emerges: the difference in the standard state reduction potentials of the eight different Highly Siderophile Elements should be sufficiently large to cause differences in metal/silicate or sulfide/silicate partition coefficients of several orders of magnitude.

6.3. Ru + RuO_2 as an Oxygen Buffer in Experimental Petrology

Figure 8 suggests that the Ru + RuO_2 equilibrium might make a useful oxygen fugacity buffer at high μO_2 (hence, very low μH_2 in hydrous systems) in high pressure experimental petrology. One advantage over alternative buffering equilibria covering a similar region of μO_2-T space (e.g., Cu_2O + CuO or CoO + Co_3O_4) is that Ru + RuO_2 remains solid even at magmatic liquidus temperatures (e.g., 1550°C at least; the melting temperature of RuO_2 is completely unknown). Another advantage is that RuO_2 will not react with silicates and shows very low solubility in silicate melts, such that the Ru + RuO_2 buffer assemblage might be mixed in directly with the experimental charge, rather than having to be segregated as in the double capsule technique. This allows buffering in dry systems. The cost of Ru and RuO_2 is not excessive when compared to those of common laboratory chemicals of reasonable purity, probably because Ru has few if any commercial uses; consequently, the use of Ru + RuO_2 as a buffer should be economically feasible. Although Ru alloys extensively with Pt, the Ru-Pt phase diagram (Massalski, 1986) does not show eutectic melting behaviour, such that extensive reaction of Ru with a Pt capsule will probably not be a problem in the timescale of a typical experimental run. Finally, the thermal expansivities and compressibilities of both Ru and RuO_2 have been measured, which, together with the molar volumes at ambient conditions (Table 2), enables accurate extrapolation of the 1 bar data for the Ru + RuO_2 equilibrium to higher pressures, using the relationship

$$\mu O_2 \equiv \Delta G^\circ_{T,P} = \Delta G^\circ_{T,1\text{bar}} + \int_{1\text{bar}}^{P} \Delta V^\circ_{\text{solids},T,P} \quad (19)$$

For Ru, we use thermal expansivities from Schröder et al. (1972) and compressibility from Clendenen and Drickamer (1964) to obtain:

$$V^\circ_{T,P}(\text{Ru}) = 0.8176[1 + 2.05 \times 10^{-5}(T - 298) - 2.94 \times 10^{-9}(T-298)^2 + 6.78 \times 10^{-12}(T-298)^3] (1 - 2.66 \times 10^{-7} P)\ \text{J bar}^{-1} \quad (20)$$

and for RuO_2, thermal expansivities from Rao and Iyengar (1969) and compressibilities from Hazen and Finger (1981) to obtain:

$$V^\circ_{T,P}(RuO_2) = 1.8865[1 + 1.45 + 10^{-5}(T - 298) + 1.53 \times 10^{-8}(T-298)^2](1 - 3.49 \times 10^{-7} P)\ \text{J bar}^{-1} \quad (21)$$

The thermal expansion measurements of Rao and Iyengar (1969a) were preferred to those of Bayer and Wiedemann (1975) as the room temperature lattice parameters determined by the former agree well with our own measurements on RuO_2 (Table 2), whereas those of Bayer and Wiedermann are significantly different (reasons unknown; the difference is extremely large compared to reasonable experimental accuracies). The temperature dependence of the compressibilities is ignored, which is customary in this type of application as such data are rarely available.

For practical applications, Eqns. 20 and 21, although a faithful rendition of the available data for the P-V-T relations of Ru and RuO_2, are unnecessarily over-precise, and the oxygen fugacity of the Ru + RuO_2 buffer can be given by the simplified expression:

$$\log_{10} f_{O_2}(\text{Ru} + RuO_2) = -16953/T + 17.98 - 2.660 \log_{10} T + 0.0562\ P/T \quad (22)$$

with negligible loss of accuracy (<0.02 log-bar units) from 700 to 1800 K and 0 to 50 kb.

An approximation to the pressure dependence of the Os + OsO_2 and Ir + IrO_2 equilibria can be made using the standard state molar volume data of Table 2.

Acknowledgments—We thank two anonymous reviewers for thorough and helpful reviews. J.N. acknowledges with gratitude the support of the Alexander von Humboldt foundation.

REFERENCES

Arblaster J. W. (1995a) The thermodynamic properties of iridium on ITS-90. *Calphad* **19,** 365–372.

Arblaster J. W. (1995b) The thermodynamic properties of osmium on ITS-90. *Calphad* **19,** 349–356.

Arblaster J. W. (1995c) The thermodynamic properties of ruthenium on ITS-90. *Calphad* **19,** 339–347.

Bannister M. J. (1984) The standard molar Gibbs free energy of formation of PbO. Oxygen concentration cell measurements. *J. Chem. Thermodyn.* **16,** 787–792.

Barin I. (1989) *Thermochemical Data of Pure Substances.* VCH Publishers.

Bayer G. and Wiedemann H. G. (1975) Formation, dissociation and expansion behaviour of platinum group metal oxides (PdO, RuO_2, IrO_2). *Thermochim. Acta* **11,** 79–88.

Bell W. E. and Tagami M. (1963) High-temperature chemistry of the ruthenium-oxygen system. *J. Phys. Chem.* **67,**

Bell W. E., Tagami M., and Inyard R. E. (1966) Dissociation of iridium oxide. *J. Phys. Chem.* **70,** 2048–2050.

Bezmen N. I., Asif M., Brügmann G. E., Romanenko I. M., and Naldrett A. J. (1994) Distribution of Pd, Rh, Ru, Jr, Os, and Au between sulfide and silicate metals. *Geochim. Cosmochim. Acta* **58,** 1251–1260.

Boman C.-E. (1970a) Refinement of the crystal structure of ruthenium dioxide. *Acta Chem. Scand.* **24,** 116–122.

Boman C.-E. (1970b) Precision determination of the crystal structure of osmium dioxide. *Acta Chem. Scand.* **24,** 123–128.

Burriel R., Westrum J. E. F., and Cordfunke E. H. P. (1987) Low-temperature heat capacity and thermodynamic functions of IrO_2. *J. Chem. Thermodyn.* **19,** 1277–1231.

Capobianco C. J. and Drake M. J. (1990) Partitioning of ruthenium, rhodium, and palladium between spinel and silicate melt and implications for platinum group element fractionation trends. *Geochim. Cosmochim. Acta* **54,** 869–874.

Chase M. W. Jr., Davies C. A., Downey J. R. Jr., Frurip D. J., McDonald R. A., and Syverud A. N. (1985). JANAF Thermochemical Tables, 3rd. edition.. *J. Phys. Chem. Ref. Data* **14,** suppl. 1

Chatterji D. and Vest R. W. (1971) Thermodynamic properties of RuO_2. *J. Amer. Ceramic Soc.* **54,** 73–74.

Clendenen R. L. and Drickamer H. G. (1964) The effect of pressure on the volume and lattice parameters of ruthenium and iron. *J. Phys. Chem. Solids* **25,** 865–868.

Clusius K. and Losa C. G. (1955) Ergebnisse der Tieftemperaturforschung. XIV. Die Atom- und Elektronenwärme des Rhodiums and Iridiums zwischen 10° and 273° K. *Z. Naturforsch* **10A,** 545–551.

Clusius K. and Piesbergen U. (1959) Ergebnisse der Tieftemperaturforschung. XXI. Atom- und Elektronenwärme des Ruthens zwischen 10 and 273° K. *Z. Naturforsch* **14A,** 23–27.

Cordfunke E. H. P. (1981) The enthalpy of formation of IrO_2 and thermodynamic functions. *Thermochim. Acta* **50,** 177–185.

Cordfunke E. H. P. and Konings R. J. M. (1988) The enthalpy of formation of RuO_2. *Thermochim. Acta* **129,** 63–69.

Cordfunke E. H. P. and Konings R. J. M. (1989) The high temperature thermophysical properties of ruthenium and palladium. *Thermochim. Acta* **139,** 99–106.

Cordfunke E. H. P., Konings R. J. M., Westrum J. E. F., and Shaviv R. (1989) The thermophysical and thermochemical properties of RuO_2 from 0 to 1000 K. *J. Phys. Chem. Solids* **50,** 429–434.

Cordfunke E. H. P. and Meyer G. (1962) The system iridium-oxygen. II. The dissociation pressure of IrO_2. *Rec. Trav. Chim.* **81,** 670–678.

Fleet M. E., Stone W. E., and Crocket J. H. (1991) Partitioning of palladium, Iridium and platinum between sulfide liquid and basalt melt: Effects of melt composition, concentration, and oxygen fugacity. *Geochim. Cosmochim. Acta* **55,** 2545–2554.

Fleet M. E., Crocket J. H., and Stone W. E. (1996) Partitioning of platinum-group elements (Os, Ir, Ru, Pt, Pd) and gold between sulfide liquid and basalt melt. *Geochim. Cosmochim. Acta* **60,** 2397–2412.

Fletcher J. M., Gardner W. E., Greenfield B. F., Holdoway M. J., and Rand M. H. (1968). Magnetic and other studies of ruthenium dioxide and its hydrate. *J. Chem. Soc. (A),* 653–657.

Franco J. I. and Kleykamp H. (1972) Freie Bildungsenthalpie von Osmiumdioxid. *Berichte der Bunsen-Gesellschaft* **76,** 691–694.

Fredrickson D. R. and Chasanov M. G. (1972) Enthalpy of ruthenium dioxide to 1200°K by drop calorimetry. *J. Chem. Eng. Data* **17,** 21–22.

Furukawa G. T., Reilly M. L., and Gallagher J. S. (1974) Critical analysis of heat-capacity data and evaluation of thermodynamic properties of ruthenium, rhodium, palladium, iridium and platinum from 0 to 300 K. A survey of the literature data on osmium. *J. Phys. Chem. Ref. Data* **3,** 163–209.

Hazen R. M. and Finger L. W. (1981) Bulk moduli and high-pressure crystal structures of rutile-type compounds. *J. Phys. Chem. Solids* **42,** 143–151.

Holland T. J. B. (1981) Thermodynamic analysis of simple mineral systems. In *Thermodynamics of Minerals and Melts* (ed. R. C. Newtonet al.), pp. 19–34. Springer-Verlag.

Jaeger F. M. and Rosenbohm E. (1932) II. La détermination exacte des chaleurs spécifiques vraies du tungstène, du rhodium, du palladium, du ruthénium, de l'osmium et de l'iridium à des températures entre 0° et 1625°C. *Rec. trav. chim.* **51,** 1–46.

Kazenas E. K., Chizhikov D. M., Bochkin L. K., and Tagirov V. K. (1974) Mass-spectrometric Study of the pressure and composition of osmium dioxide vapour. *Russ. J. Inorg. Chem.* **19,** 1418–1419.

Kleykamp H. (1969) Bestimmung der freien Bildungsenthalpie von Rutheniumdioxid mit einer galvanischen Festkörperkette. *Z. Physikal. Chemie (n.f.)* **66,** 131–136.

Kleykamp H. and Paneth L. J. (1973) Gibbs energy of formation of iridium dioxide. *J. inorg. nucl. Chem* **35,** 477–482.

Mallika C. and Sreedharan O. M. (1990) Standard Gibbs energies of formation of $RuO_2(s)$ and $LaRuO_3(s)$ by oxide e.m.f. measurements. *J. Less-Common Metals* **162,** 51–60.

Mallika C., Sreedharan O. M., and Chandrasekharaiah (1985) Determination of the standard Gibbs energy of formation of $Rh_2O_3(s)$ and $IrO_2(s)$ from solid oxide electrolyte electromotive force measurements. *J. Less-Common Metals* **107,** 203–212.

Massalski T. B. (1986) *Binary alloy phase diagrams.* Amer. Soc. Metals, Ohio.

Mattioli G. S. and Wood B. J. (1988) Magnetite activities across the $MgAl_2O_4$-Fe_3O_4 spinel join, with application to thermobarometric estimates of upper mantle oxygen fugacity. *Contrib. Mineral Petrol.* **98,** 148–162.

Naumov V. N., Paukov I. E., Ramanauskas G. R., and Chekhovskoi V. Y. (1988) Specific heat and thermodynamic functions of osmium at 5-316 K. *Russ. J. Phys. Chem.* **62,** 12–15.

Naumov V. N., Paukov I. E., and Sukhovei K. S. (1991) Thermodynamic properties of ruthenium at 6-310 K. *Russ. J. Phys. Chem.* **65,** 121–123.

Nell J. and O'Neill H. St.C. (1996) Gibbs free energy of formation and heat capacity of PdO: A new calibration of the Pd-PdO buffer to high temperatures and pressures. *Geochim. Cosmochim. Acta* **60,** 2487–2493.

Nell J. and O'Neill H. St.C. (1997) The Gibbs free energy of formation and heat capacity of β-Rh_2O_3 and "$MgRh_2O_4$", the MgO-Rh-O phase diagram, and constraints on the stability of $Mg_2Rh^{4+}O_4$. *Geochim. Cosmochim. Acta* **61,** 4159-4171.

Nikol'ski A. B., Semenov G. A. and Veshnyakova E. N. (1967) The thermal decomposition of osmium dioxide. *Russ.J. Inorganic Chem.* **12,** 571.

O'Neill H. St.C. (1986) The Mo-MoO_2 (MOM) oxygen buffer and the free energy of formation of MoO_2. *Amer. Mineral.* **71,** 1007–1010.

O'Neill H. St.C. (1988) Systems Fe-O and Cu-O: thermodynamic data for the equilibria Fe- "FeO", Fe-Fe_3O_4, "Fe-O" -Fe_3O_4, Fe_3O_4-Fe_2O_3, Cu-Cu_2O, and Cu_2O-CuO from emf measurements. *Amer. Mineral.* **73,** 470–486.

O'Neill H. St. C. and Pownceby M. I. (1993) Thermodynamic data from redox reactions at high temperatures. I. An experimental and theoretical assessment of the electrochemical method using stabilized zirconia electrolytes, with revised values for the Fe-"FeO", Co-CoO, Ni-NiO and Cu-Cu_2O oxygen buffers, and new data for the W-WO_2 buffer. *Contrib. Mineral. Petrol.* **114,** 296–314.

O'Neill H. St. C., Dingwell D. B., Borisov A., Spettel B., and Palme H. (1995) Experimental petrochemistry of some highly siderophile elements at high temperatures, and some implications for core formation and the mantle's early history. *Chem. Geol.* **120,** 255–273.

Pankratz L. B. (1982) *Thermodynamic Properties of Elements and Oxides.* US Bureau of Mines.

Peach C. L., Mathez, E.A., and Keays, R.R. (1990) Sulfide melt–silicate melt distribution coefficients for noble metals and other chalcophile elements as deduced from MORB: Implications for partial melting. *Geochim. Cosmochim. Acta* **54,** 3379–3389.

Peach, C. L., Mathez, E.A., Keays, R.R., and Reeves, S.J. (1994) Experimentally determined sulfide melt–silicate melt partition coefficients for iridium and palladium. *Chem. Geol.* **117,** 361–377.

Pizzini S. and Rossi L. (1971) Thermodynamics of the system ruthenium-oxygen. Determination of the free energy of formation of RuO_2 by means of emf measurements. *Z. Naturforsch.* **26a,** 177–179.

Pownceby M. I. and O'Neill H. St.C. (1994) Thermodynamic data from redox reactions at high temperatures. IV. Calibration of the Re-ReO_2 oxygen buffer from EMF and NiO + Ni-Pd redox sensor measurements. *Contrib. Mineral. Petrol* **118,** 130–137.

Ramakrishnan E. S., Sreedharan O. M., and Chandrasekharaiah M. S. (1975) The free energy of formation of iridium oxide by solid electrolyte galvanic cell. *J. Electrochem. Soc.* **122,** 328–331.

Ramanauskas G., Chekhovskoi V. Y., Tarasov V. D., Shishkov V. V., and Koltygin V. M. (1987) The enthalpy of single crystal iridium in the high temperature range. *Russ. J. Phys. Chem.* **61,** 742–743.

Ramanauskas G. R., Tarasov V. D., Chekhovskoi V. Y., Korenovskii N. L., and Polyskova V. P. (1988) High-temperature enthalpy of vacuum-melted ruthenium and osmium. *High-Purity Substances* **4,** 688–691.

Rao K. V. K. and Iyengar L. (1969a) X-ray studies on the thermal expansion of ruthenium dioxide. *Acta Cryst.* **A25,** 302–303.

Rao K. V. K. and Iyengar L. (1969b) Thermal expansion of iridium dioxide. *Current Science* **13,** 304–305.

Robie R. A., Hemingway B. S. and Fisher J. R. (1978) Thermodynamic properties of minerals and related substances at 298.15 K and 1 bar (10^5 pascals) pressure and higher temperatures. *USGS Bull.* 1452.

Rogers D. B., Shannon R. D., Sleight A. W., and Gillson J. L. (1969) Crystal chemisty of metal dioxides with rutile-related structures. *Inorg. Chem.* **8,** 841–849.

Schäfer H. and Heitland H.-J. (1960) Gleichgewichtsmessungen im System Iridium-Sauerstoff. Gasförmiges Iridiumtrioxyd. *Z. anorg. allg. Chem.* **304,** 249–265.

Schäfer H., Schneidereit G. and Gerhardt W. (1963) RuO_2 Chemischer Transport, Eigenschaften thermischer Zerfall. *Z. anorg. allg. Chem.* **319,** 327–336.

Schröder R. H., Schmitz-Pranghe N., and Kohlhaas R. (1972) Experimentelle Bestimmung der Gitterparameter der Platinmetalle im Temperaturbereich von - 190 bis 1709°C. *Z. Metallk.* **63,** 12–16.

Shchukarev S. A. and Ryabov A. N. (1960) Heat of formation of ruthenium dioxide. *Russ. J. Inorg. Chem.* **5,** 941–942.

Singh H. P. (1968) Determination of Thermal expansion of germanium, rhodium, and iridium by X-rays. *Acta Cryst* **A24,** 469–471.

Tagirov V. K., Chizhikov D. M., Kazenas E. K., and Shubochkin L. K. (1975) Thermal dissociation of ruthenium dioxide and rhodium sesquioxide. *Russ. J. Inorganic Chem.* **20,** 1133–1135.

Zador S. (1967) Non-stoichiometric Measurements in Dioxides of the Rutile Structure. In *Electromotive Force Measurements in High-temperature systems* (ed. C. B. Alcock); *Proceedings of symposium held by the Nuffield Research Group, Imperial College, London,* pp. 145–150. The Institution of Mining and Metallurgy, Portland Place, London.